ON THE DYNAMIC MODELING OF AN ARTICULATED ELECTROHYDRAULIC FORESTRY MACHINE

Evangelos Papadopoulos and Soumen Sarkar

Department of Mechanical Engineering & Centre for Intelligent Machines
McGill University
Montreal, PQ, Canada H3A 2A7
egpapado@cim.mcgill.edu

Abstract

This paper focuses on the generation of dynamic models for an electrohydraulic forestry machine. Such models can be used for training simulators, for sizing components, and for system design. The most complex model includes base compliance, and pendulum-like motions of the processing head suspended from an end-point. A Newton-Euler iterative method, implemented symbolically, is used to include base degrees-of-freedom due to the machine's compliant tires. Techniques and experiments designed to extract system parameters are described. Based on the obtained models, a valve-sizing methodology is briefly outlined. Finally, simulation results of the machine's response are provided.

1 Introduction

Forestry is Canada's most important industry in terms of net contribution to its economy [1]. However, competition from overseas and new environmental laws require that forestry resources are harvested more efficiently and more carefully than previously. This requires more sophisticated forestry equipment that is appropriate to available forests, and that allows for increased harvesting capacity with less damage to the soil and the trees, and for selective logging. At the same time, such equipment should be easier to control and less tiring, so that operators can focus in planning the local operation better.

Many of these requirements can be met by the addition of an on-board information system that can be used for assisting repetitive tasks, for diagnosing the state of the machine, and most importantly, for controlling it. The availability of cost-effective industrial grade computers, and actuator-sensor mechatronic packages that can withstand the harsh forestry environment, make such "computerization" of forestry machines possible. In fact, some North-American and Scandinavian forestry machines already incorporate some of these systems. For example there exist harvesters which also cut logs to pre specified lengths using opto-electronic or mechanical measurements of log length and diameter.

Many of the existing felling machines are modified construction machines, usually large excavators. Typical modifications include geometrical modifications for better workspace utilization, and addition of specialized processing heads, controlled from the cabin with separate interfaces. Work on coordinated control of excavator-type of machines has began in mid-eighties by P.D. Lawrence and his team [2,3]. In this work, an excavator end-point is controlled in cylindrical task space coordinates by an operator rotating with the arm and using a single joystick. However, an important trend in forestry equipment is designing machines for the environment they work in. Such machines should have the appropriate workspace size and shape, be lightweight, be maneuverable, and agile. In contrast to excavator machines, the operator of a machine designed for forestry operations may be sitting in a non-moving cabin, and commanding the manipulator in Cartesian space. In addition, actuation systems for such machines are being improved. For increased speed of response, new systems are increasingly based on fast closed-center proportional valves, and constant pressure supplies.

This paper reports preliminary work focusing on the modeling and control of an experimental forestry machine. Detailed dynamical models at various degrees of complexity are developed to help in designing effective coordinated controllers in Cartesian space, and in developing a training simulator for novice operators. A Newton-Euler iterative method, implemented symbolically, is used to include base degrees-of-freedom (dof) due to the machine's compliant tires. The models also include pendulum-type motions of the suspended processing head.

These models differ from standard dynamical models developed in robotics primarily because some of the system degrees-of-freedom are either not actuated, or affected by passive spring-damper suspensions. Parameters for these models were obtained from drawings, actual measurements, simple experiments, and solid modeling techniques. As an application of the developed dynamical models, a valve sizing methodology is briefly outlined. Finally, the paper concludes with simulation results of the response of the system in manipulator commands.

2 Overview of the FERIC Experimental Machine

The work described in this paper is part of a recent Canadian initiative in forestry robotics, called 'ATREF' (Application des Technologies Robotiques aux Équipements Forestiers). This is a four-year $2.2M project which began in 1994, and involves industrial and university partners [4]. For the needs of this project, one of the partners, FERIC, has contributed a side-loading forwarder, see Figure 1. This machine consists of an articulated base that can adjust one degree-of-freedom (its pitch) by means of a hydraulic piston. Due to a special base articulation system, the two base bogies can move with respect to each other, so as to minimize base pitch and roll. The machine is equipped with an articulated manipulator arm which includes a swing joint, actuated by a hydraulic motor, and boom and stick joints, actuated by hydraulic cylinders. At the stick end-point, a Hooke-type assembly permits free swinging of the processing head in two dofs.

To improve operator visibility, machine stability, and workspace, the original experimental machine, shown in Figure 1, was modified by relocating the cabin and manipulator. Manipulator structural modifications were also necessary to increase the workspace area proximal to the ground. Kinematic modeling of the arm and plotting of its reachable workspace confirmed that lengthening of the stick had the desired effect.

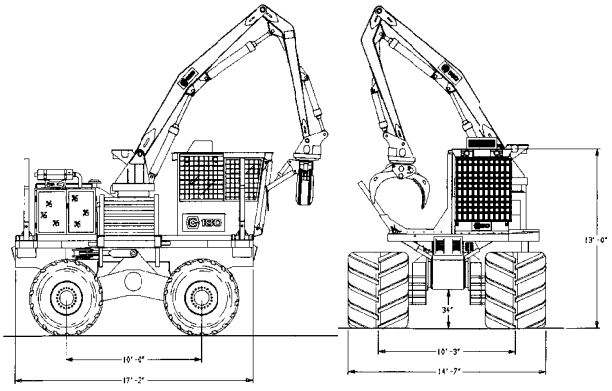

Figure 1. The FERIC Experimental Machine.

Indeed, as shown in Figure 2, the new workspace is more flat and extended along a horizontal surface at its lower end. With the eventual replacement of the grapple by a specialized end-effector attachment, the machine will be transformed from a side-loader to a wood-harvester [4].

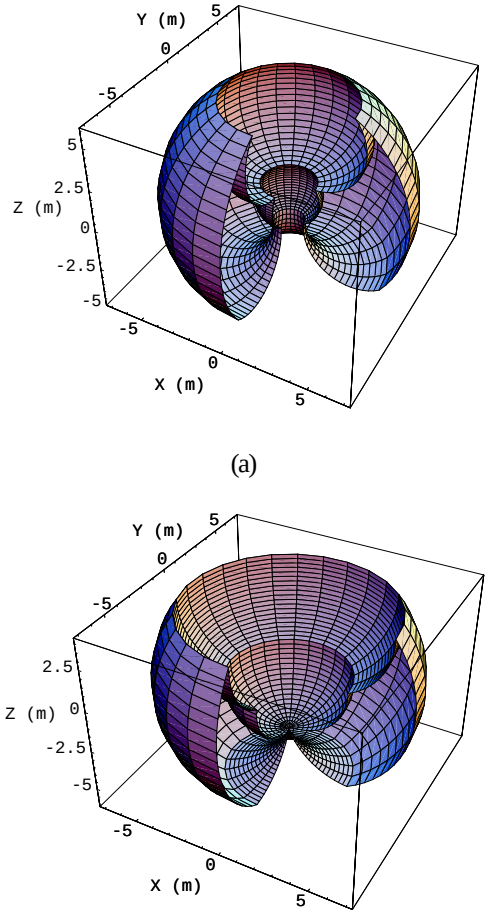

(a)

(b)

Figure 2. The reachable workspace of the manipulator with (a) short stick, (b) long stick.

Traditional manipulation control in forestry and construction machines is based on open-loop joint control, i.e. the operator is controlling separately each joint of the arm, and mentally coordinates the motion of the arm's end-effector in Cartesian space. Motion errors due to hardware limitations are partly compensated by the operator, depending on skill and experience. Computerized coordinated control can reduce operator workload by assigning the coordination task to an on-board computer. However, compensation for errors requires responsive actuation and control systems. While the original electro-hydraulic system of the FERIC machine reflected traditional industry practice, careful analysis suggested that

the benefits of computerized control would be limited without changes to certain electro-hydraulic components. In particular, to improve responsiveness and joint coordination, it was decided to replace the original load-sensing actuation valves with proportional valves working with a constant pressure supply. As a result, finer filters were installed to address stricter oil filtering requirements.

For the purposes of control and identification experiments, the machine was equipped with magnetostrictive sensors (measuring cylinder displacement), resolvers (measuring angles), inclinometers (measuring vehicle orientation), and flow and pressure sensors for the hydraulics related experiments. These sensors also proved helpful in debugging the hardware. More details about the machine modifications and the on-board sensors can be found in Reference [4].

3 Dynamic Modeling

In contrast to conventional industrial manipulators which are mounted on fixed bases, a mobile manipulator is mounted on a moving and compliant base. The non-fixed base introduces additional system dofs. However, the dofs associated with base compliance, are not actuated. These characteristics introduce additional complexity to the dynamic modelling and control of such systems.

In the study of system dynamics, we consider the forces and/or torques required to cause motion of manipulator. A number of methods are available to formulate manipulator dynamics, including the iterative Newton-Euler dynamic formulation, the Lagrangian formulation, Kane's method, and others. For the needs of this work, the iterative Newton-Euler dynamic formulation was chosen because it is easy to implement in the form of computer code, and it requires a smaller number of computations [5,6]. In general, in this method kinematic quantities are calculated with outward computations starting from the base and ending at the tip, while actuator forces and torques are computed with inward computations. Gravity forces are included by simply assuming that the base frame is accelerated upwards with an acceleration equal to that of gravity.

However, the iterative Newton-Euler algorithm was developed for fixed-base systems in which all dofs are actuated. In such case, known desired trajectories for all joints, or dofs, are used to calculate numerically the forces and torques necessary to cause the desired motion. This is not possible in the case of a manipulator mounted on a compliant base, since the base is not actuated, and its position, velocity and acceleration will depend on how fast the arm moves, the load being manipulated, etc. However, if this formulation is applied symbolically, then it results in a closed set of symbolic equations of motions, which is not subject to this problem. This is the approach taken here, and is explained in detail below.

The vehicle and all other sub-systems excluding the manipulator, are modeled as a lumped mass, called thereafter as the 'base', see Figure 3. The base may oscillate around its home position, but it will not translate, i.e. the wheels are assumed locked. A body fixed frame 0 is attached to the base, that coincides with a world-fixed frame when the vehicle is at its home position. The $\hat{x}_0$ axis of the body-fixed frame is along the direction of forward motion of the vehicle, while at home position, its $\hat{z}_0$ axis is in opposite direction to the gravity vector.

A force/torque set, (*f*, *n*), is applied to the base through the tires and the ground. Here it is assumed that the soil has been compacted, and that most of the base compliance is due to the machine's pneumatic tires. Therefore, these forces depend on the state of the tires. The four tires of the forestry vehicle are modeled as four parallel springs and dampers. The simultaneous vertical motion of the springs gives rise to a bouncing effect of the system. Due to the parallel spring structure, the base is also subject to pitch (rotation of the base around the $\hat{y}_0$ axis) and roll (rotation of the base around the $\hat{x}_0$ axis) motions. For small deviations from the home position, the yaw effects are negligible, and are therefore neglected. There are five links in the manipulator namely (from base to tip) the swing, boom, stick, pin and end-effector. The last two links are not actuated but instead they are connected with free joints, and hence a load attached to the last link swings like a double pendulum (gimbals).

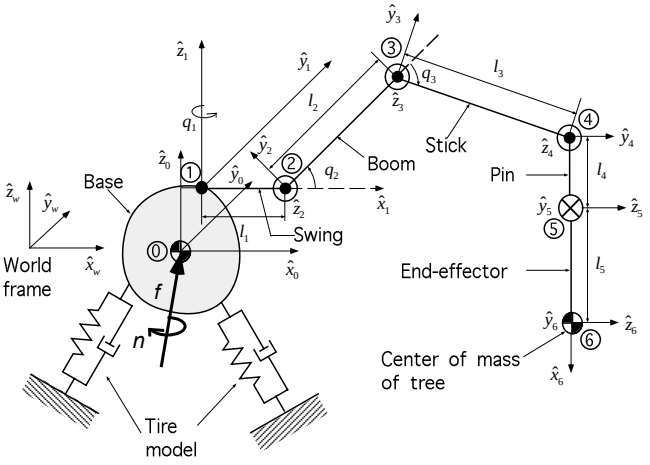

Figure 3. The 8 dof system model, and associated frames.

On all five links, frames are attached following the modified Denavit-Hartenberg methodology as described in [7], see Figure 3. Frame 0, i.e. the base frame $(\hat{x}_0\hat{y}_0\hat{z}_0)$, is attached at the center of mass of the base and has the same orientation with the swing frame, when the angle of rotation is zero. The rotation matrix that transforms vector in the base frame to ones in the world frame is computed based a zyx Euler angle succession and is given by

$$ {}^{w}R_0 = \begin{bmatrix} c_z & -s_z & 0 \\ s_z & c_z & 0 \\ 0 & 0 & 1 \end{bmatrix} \begin{bmatrix} c_y & 0 & s_y \\ 0 & 1 & 0 \\ -s_y & 0 & c_y \end{bmatrix} \begin{bmatrix} 1 & 0 & 0 \\ 0 & c_x & -s_x \\ 0 & s_x & c_x \end{bmatrix} \quad (1) $$

where c_z is the cosine of q_z and s_z is the sine of q_z, etc. The angles q_x, q_y, and q_z are the roll, pitch and yaw respectively. Since the yaw is neglected, q_z is set equal to zero and this rotation matrix becomes,

$$ {}^{w}R_0 = \begin{bmatrix} c_y & 0 & s_y \\ 0 & 1 & 0 \\ -s_y & 0 & c_y \end{bmatrix} \begin{bmatrix} 1 & 0 & 0 \\ 0 & c_x & -s_x \\ 0 & s_x & c_x \end{bmatrix} \quad (2) $$

The position vectors are shown below

$$ {}^{w}p_0^{w} = \begin{bmatrix} x_w \\ y_w \\ z_w \end{bmatrix}, \; {}^{0}p_1^{0} = \begin{bmatrix} x_0 \\ y_0 \\ z_0 \end{bmatrix}, \; {}^{0}p_{c_0}^{0} = \begin{bmatrix} 0 \\ 0 \\ 0 \end{bmatrix} \quad (3) $$

where the symbol ${}^{a}p_c^{b}$ should be read as the position vector of the point *c* with respect to frame *b* expressed in frame *a*. The initial conditions for the iterative Newton-Euler methodology are given below

$$ {}^{w}v_w = \begin{bmatrix} 0 \\ 0 \\ 0 \end{bmatrix}, \; {}^{w}\dot{v}_w = \begin{bmatrix} 0 \\ 0 \\ g \end{bmatrix}, \; {}^{w}\omega_w = \begin{bmatrix} 0 \\ 0 \\ 0 \end{bmatrix}, \; {}^{w}\dot{\omega}_w = \begin{bmatrix} 0 \\ 0 \\ 0 \end{bmatrix} \quad (4) $$

Applying velocity and acceleration propagation equations, and assuming that yaw is zero, we obtain

$$ {}^{0}\omega_0 = {}^{0}R_w \, {}^{w}\omega_w + \begin{bmatrix} \dot{q}_x \\ \dot{q}_y \\ 0 \end{bmatrix} = \begin{bmatrix} \dot{q}_x \\ \dot{q}_y \\ 0 \end{bmatrix} \quad (5) $$

Only the vertical bounce effect is considered so,

$$ {}^{0}v_0 = {}^{0}R_w \left({}^{w}v_w + {}^{w}\omega_w{}^{\times \, w}p_0^{w} \right) + \begin{bmatrix} 0 \\ 0 \\ \dot{z} \end{bmatrix} = \begin{bmatrix} 0 \\ 0 \\ \dot{z} \end{bmatrix} \quad (6) $$

$$ {}^{0}\dot{v}_0 = {}^{0}R_w \left[{}^{w}\dot{v}_w + {}^{w}\dot{\omega}_w{}^{\times \, w}p_0^{w} + {}^{w}\omega_w{}^{\times} \left({}^{w}\omega_w{}^{\times \, w}p_0^{w} \right) \right] + 2 \left({}^{0}R_w \, {}^{w}\omega_w \right)^{\times} \begin{bmatrix} 0 \\ 0 \\ \dot{z} \end{bmatrix} + \begin{bmatrix} 0 \\ 0 \\ \ddot{z} \end{bmatrix} \quad (7) $$

$$ {}^{0}\dot{v}_{c_0} = {}^{0}\dot{v}_0 + {}^{0}\dot{\omega}_0{}^{\times \, 0}p_{c_0}^{0} + {}^{0}\omega_0{}^{\times} \left({}^{0}\omega_0{}^{\times \, 0}p_{c_0}^{0} \right) = {}^{0}\dot{v}_0 \quad (8) $$

$$ {}^{0}F_0 = m_0 \, {}^{0}\dot{v}_{c_0} \quad (9) $$

$$ {}^{0}N_0 = {}^{0}I_0^{c} \, {}^{0}\dot{\omega}_0 + {}^{0}\omega_0{}^{\times} \, {}^{0}I_0^{c} \, {}^{0}\omega_0 \quad (10) $$

where the subscript $^{\times}$ converts a vector to the corresponding skew-symmetric cross-product matrix, m_0 and ${}^{0}\dot{v}_{c_0}$ are the mass of the base and acceleration of the center of mass of the base expressed in base frame, i.e. frame 0. The inertia tensor of the *i*th link with respect to a frame located at the center of mass of the *i*th link with same orientation of *i*th frame is denoted by ${}^{i}I_i^{c}$. The symbols ${}^{i}F_i$ and ${}^{i}N_i$ denote the force and moment acting at the center of mass of the *i*th link expressed in the *i*th frame.

The complete algorithm for computing joint torques from the motion of the joints is composed of two iterations. During the forward iteration, link velocities and accelerations are iteratively computed form link 1 to link 5 and the Newton-Euler equations are applied to each link. During the backward iteration, constraint forces and torques, and joint actuator torque are computed recursively from link 5 to link 1. A more detailed description of this part of the iterations can be found in [7]. The forces and torques transmitted to the base by the manipulator can then be found using the following equations

$$ {}^{0}f_0 = {}^{0}R_1 \, {}^{1}f_1 + {}^{0}F_0 \quad (11) $$

$$ {}^{0}n_0 = {}^{0}N_0 + {}^{0}R_1 \, {}^{1}n_1 + {}^{0}p_{c_0}^{0\,\times} \, {}^{0}F_0 + {}^{0}p_1^{0\times} \, {}^{0}R_1 \, {}^{1}f_1 \quad (12) $$

where the symbols ${}^{i}f_i$ and ${}^{i}n_i$ denote the force and torque exerted on link *i* by link *i*-1, expressed in frame *i*. The force and torque vectors at the center of mass of the base (${}^{0}f_0$ and ${}^{0}n_0$) can be found out as a last component of the inward iterations as shown in Eq. (11) and Eq. (12). This forces and torque can be expressed in world frame as follows

$$ {}^{w}f_0 = {}^{w}R_0 \, {}^{0}f_0 \quad (13) $$

$$ {}^{w}n_0 = {}^{w}R_0 \, {}^{0}n_0 \quad (14) $$

where ${}^{w}R_0$ can be found from Eq. (2). Introducing a generalized force vector *(F)*,

$$F = \begin{bmatrix} {}^{w}f_0 \\ {}^{w}n_0 \end{bmatrix} \tag{15}$$

Vector F can be equated with forces and torques generated by the tires, as follows

$$F = -KX - B\dot{X} \tag{16}$$

where X and $\dot{X}$ are generalized displacement and velocity vectors with respect to world frame. K and B are the stiffness and damping matrices and capture the effect of the tire model. For simplicity, and for small motions, these matrices are assumed to be diagonal

$$K = diag\left(k_x, k_y, k_z, k_1, k_2, k_3\right) \tag{17}$$

$$B = diag\left(b_x, b_y, b_z, b_1, b_2, b_3\right) \tag{18}$$

The symbols k_x, k_y and k_z represent the total linear stiffnesses along the corresponding directions, as denoted by subscript with respect to the world frame. The term 'total' stiffness is used to represent the combined stiffness of the four tires. The other parameters k_1, k_2 and k_3 represent the total angular stiffness namely roll, pitch and yaw (rotation with respect to $\hat{x}_w, \hat{y}_w$ and $\hat{z}_w$ as experienced at the center of mass of the base). The same notation is applied in case of damping. Since only three base motions are considered important, i.e., bounce, roll and pitch, the remaining base equations are dropped. When this is done, the other two displacements are constant and the yaw angle is zero.

Finally, the equations of motion are written as

$$M\ddot{q} + V(q,\dot{q}) + G(q) = \tau \tag{19}$$

where M is an 8×8 symmetric and positive definite mass matrix, V contains the Coriolis and centrifugal terms, G the gravity terms and τ is the force/torque vector. A reduced five dof order model is formed by neglecting base compliance in the eight dof model. This model will be used as the dynamics engine of a real-time training simulator also undergoing development as part of the ATREF project [8]. A further reduced model of three dofs, formed by neglecting the Hooke-type gimbals, has been used for the valve sizing studies, described in Section 5.

4 Parameter Estimation

Model parameters are needed to run the simulations, validate the developed code, and design controllers. Geometrical parameters such as lengths can be found from blueprints, and verified by direct measurements. Some masses are also found from drawings, or by directly weighing the body of interest. But the parameters like center of mass locations, and moments and products of inertia, can not be obtained from drawings. In the case of the boom and stick, pendulum experiments were carried out to measure the moments of inertia of those links. In the case of products of inertia no such experiments can be made easily. For these, solid modeling techniques and the Advanced Modeling Extension package of AutoCAD were used. Another set of parameters was required to characterize the base compliance due to the tires. The stiffness and damping ratio of the tires are found by static load-deflection tests and drop tests, respectively.

4a. Pendulum Experiments

Pendulum experiments are not always possible, because they require disassembling a system to its components. In this case, it was possible to do them while the machine was disassembled for maintenance reasons. During a pendulum experiment, a rigid body is first suspended from a point, usually one of its joints. After the body comes to a rest, it is angularly displaced with respect to some axis, and then it is set free to swing. The period of the resulting oscillation is recorded, and is subsequently used to calculate the moment of inertia around the axis of rotation according to the following equation

$$\omega = \frac{2\pi}{T} = \sqrt{\frac{mgl}{I_{zz}^{o}}} \tag{20}$$

where I_{zz}^{0} is the moment of inertia of the rigid body with respect to the axis of swinging (generally denoted as a z-axis), ω is the natural frequency of the oscillation, T is the period of oscillation, l is the length from the point of suspension to the center of mass of the body, and m is the mass of the body. Rearranging the terms we get,

$$I_{zz}^{0} = \frac{mglT^2}{4\pi^2} \tag{21}$$

Since the Newton-Euler formulation requires that the moment of inertia is expressed with respect to the center of mass of the body, the parallel axis theorem is employed as follows

$$I_{zz}^{c} = I_{zz}^{o} - ml^2 \tag{22}$$

As revealed by Eq. (21), the inertia is proportional to the square of the time period. Therefore, errors in obtaining the period of oscillation may result in substantial errors in calculating the moment of inertia. Moreover, swinging a body with respect to a single axis is a difficult task. For these reasons, pendulum experiments are not absolutely satisfactory for obtaining moments of inertia. The accuracy of these estimates can be improved by a combination of experiments and solid modeling techniques.

4b. Solid Modeling

Solid modeling techniques can be used in obtaining all mass properties and center-of-mass positions, assuming that the material and the geometry of a body or link are precisely known. However, this is not always the case. To match solid modeling estimates to measurements, links of interest were weighted, and some moments of inertia were calculated using pendulum experiments. Then, solid models were refined to the point that both the estimated and measured total mass and moment of inertia were in agreement.

The basic concept in solid modeling requires that first a closed boundary should be drawn around a two dimensional surface, and then that this boundary is extracted to a certain height with appropriate taper angles to result in a solid body. To create body holes or cavities, another body is created with the shape of the required hole and it is subtracted from the original one. Once the solid model is positioned and oriented with respect to a frame, special routines calculate the body's mass properties with respect to this frame. The solid models generated for the swing and the boom are shown in Figure 4.

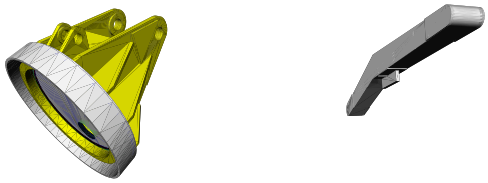

Figure 4. Solid models generated in AutoCad.

Following the techniques described above, the inertia parameters of the main links were obtained and are given in Table I.

Table I. Link Inertia Properties.

in kgm^2	I_{xx}	I_{yy}	I_{zz}	I_{xy}	I_{yz}	I_{zx}
Swing	52	53	56	.01	.02	5
Boom	17	926	929	.36	-.09	-.70
Stick	16	816	826	32	.14	.51
Pin	0	3.3	3.3	0	0	0
End-eff.	0	1265	1265	0	0	0

4c. Load-deflection Experiment

To obtain the tire stiffness, k, load-deflection experiments were conducted. In these, a load is applied on a tire and its vertical deflection is measured. Figure 5 shows a typical plot obtained from such experiment. As shown by this figure, the tire behaves like a linear spring in the region of loads of interest. From the average slope of the plot in Figure 5, the tire stiffness was computed as equal to $k = 49.23\ kg/mm$. This stiffness allows us to calculate the translational and angular stiffness for bounce, roll and pitch using geometrical expressions.

4d. Drop Experiment

One of the simplest methods to estimate the damping ratio of a non-rolling tire is the so-called drop test. The experimental procedure for standard automotive tires is described in [9]. In the case of a light tire, a load is added to the hub of the tire, which is just in contact with a steel slab, without deforming it (the load is supported externally). The load is then set free, and the loaded tire is allowed to deform freely from its initial position. Throughout the test, the tire must be in contact with the slab, otherwise obtained results will not be valid due to the physics of the collisions. An accelerometer mounted on its hub records the tire transient response, which corresponds to an underdamped oscillation. Figure 6 displays a typical accelerometer reading during a drop experiment.

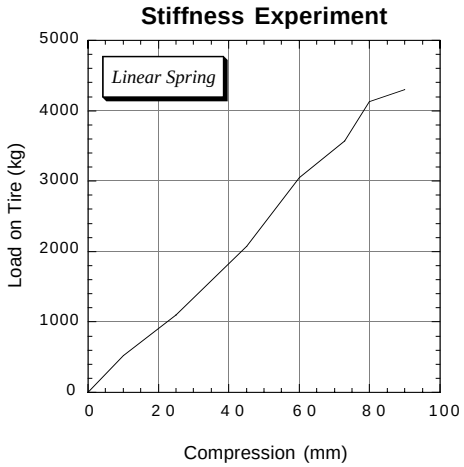

Figure 5. Results of a tire stiffness experiment.

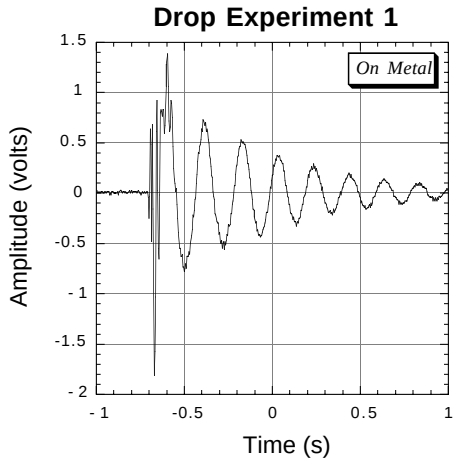

Figure 6. Accelerometer reading for tire damping estimation.

Double integration of the acceleration data such as the one displayed in Figure 6, yields the hub time response. Then, using the amplitude of two successive periods of the response, x_1 and x_2 and the logarithmic decrement equation, the damping ratio coefficient, ζ, is found according to

$$\ln\left(\frac{x_1}{x_2}\right) = \frac{2\pi\zeta}{\sqrt{1-\zeta^2}} \tag{23}$$

The value of the damping ratio from the experiment is computed as 0.035. Based on this estimate, and on the mass of the tire, the tire damping coefficient is calculated. The damping coefficient for the pitch, roll, and bounce can then be found easily [6].

5 Valve Sizing Based on Inverse Dynamics

An important application of the dynamic modeling is sizing of actuators. In the case of the experimental electrohydraulic machine, it has been decided not to replace the existing boom and stick hydraulic cylinders and the swing motor. However, the need to select new constant-pressure proportional valves to replace the old load-sensing ones provided the first application for the derived dynamical models. According to typical industrial practice, proportional valves are selected based on a nominal load and duty cycle. However, no such nominal quantities exist for a manipulator arm whose configuration changes continuously, and may carry no load, or be loaded with a heavy tree. Therefore, a systematic methodology for valve sizing is needed.

A valve is properly sized when it can supply the demanded flow at the required pressure drop across it. Therefore to size a valve, flow and pressure requirements must be obtained as a function of time for a given task. Obviously, the task becomes more demanding when the manipulator is moving a heavy payload, or when it operates on a slope.

To this end, typical average as well as worst-case trajectories of the manipulator end-point were specified by observation of actual forestry machines. Using inverse kinematics relationships, these end-point trajectories were resolved at the actuator level, to result in trajectories for the swing angle, and the boom and stick displacements. Then, these can be used to obtain the flow requirements for all three actuated dofs.

Assuming average piston areas, the flow through the stick valve and cylinder is

$$Q_{stick} = A_s \dot{x}_s \tag{24}$$

where A_s is the area of the stick cylinder, and $\dot{x}_s$ is the velocity of the stick piston, a nonlinear function of the corresponding joint velocity. Similarly, the flow through the boom valve and cylinder is

$$Q_{boom} = A_b \dot{x}_b \tag{25}$$

where A_b is the area of the boom cylinder, and $\dot{x}_b$ is the velocity of the boom piston. Since the swing is driven by a gear motor, the flow through the swing motor valve is

$$Q_{swing} = D\, n\, \dot{q}_1 \tag{26}$$

where D is the motor displacement, n is the gear ratio from the swing to swing motor, and $\dot{q}_1$ is the angular velocity of the manipulator swing.

To obtain the pressure drops through the three valves, a reduced three dof dynamic model that includes the actuated dofs (swing, boom, stick) was used. From this model and the desired trajectories, the necessary forces at the two cylinders, and the torque necessary to rotate the manipulator were computed using inverse dynamics equations in the form of Eq. (19). These forces and torques are related to the pressure drops Δp at the cylinders and the swing motor according to the following equations

$$\Delta p_{stick} = \frac{f_{stick}}{A_s} \tag{27}$$

$$\Delta p_{boom} = \frac{f_{boom}}{A_b} \tag{28}$$

$$\Delta p_{swing\ motor} = \frac{\tau_{swing\ motor}}{D} = \frac{\tau_{swing}}{nD} \tag{29}$$

where f_{stick} is the force applied by the stick cylinder, f_{boom} is the force applied by the boom cylinder, and $\tau_{\text{swing motor}}$ is the torque applied by the hydraulic motor. Neglecting line

pressure drops, the pressure drop at the valves is then given by

$$\Delta p_{v,stick} = p_{op} - \left|\Delta p_{stick}\right| \tag{30}$$

$$\Delta p_{v,boom} = p_{op} - \left|\Delta p_{boom}\right| \tag{31}$$

$$\Delta p_{v,swing\ motor} = p_{op} - \left|\Delta p_{swing\ motor}\right| \tag{32}$$

where p_{op} is the constant operating pressure of the machine's pumps. If necessary, these estimates can be decreased by a 10% factor to allow for pressure drops in the transmission lines. Equations (24-26) and (30-32) can be used to plot valve flow versus valve drop for the desired end-point trajectories. The resulting Q-Δp curve should lie below the valve pressure-flow characteristic, Q_v-Δp_v, typically a curve described by a relationship of the form,

$$Q_v = c\sqrt{\Delta p_v} \tag{33}$$

If this is not the case, a valve of larger capacity must be specified. Figure 7 shows typical plots of such curves for the boom, stick, and swing, when the base is working on a sloped terrain, i.e. the base is tilted with respect to the $\hat{x}_0$ axis by 20^o (see Figure 3). Since all plots lie under the valve characteristic, this valve can be used for driving all manipulator actuators along the desired trajectory.

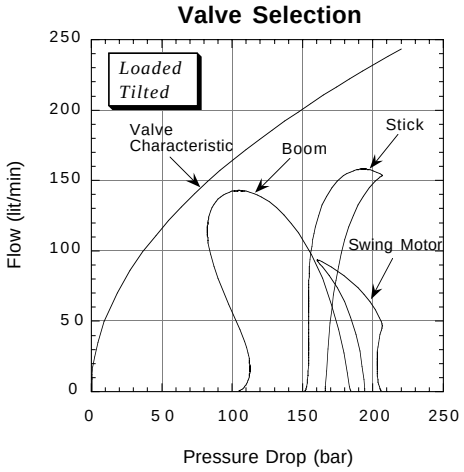

Figure 7. Valve sizing requires that boom, stick and swing pressure-flow plots lie below the valve characteristic.

Note that the dynamic models obtained permit also either sizing of the system power supply (pumps) or checking whether the desired trajectory can be followed without exceeding the power capacity of the supply. The total power requirement is the sum of all individual power requirement for the powered joints. For example the power required for stick is given by

$$P_{stick} = \left|\tau_{stick}\,\dot{q}_3\right| = \left|f_{stick}\,\dot{x}_s\right| \tag{34}$$

where τ_{stick} is the torque required to move the stick at an angular velocity of $\dot{q}_3$. Obviously, the total power required for a given trajectory can be obtained by

$$P_{total} = P_{swing} + P_{boom} + P_{stick} + P_{losses} \tag{35}$$

Based on the above equations, the total power, flow and all other variables can be plotted against time to permit easy evaluation of the system performance and requirements.

6 Dynamic Response using Forward Dynamics

In this section the dynamic behavior of the eight dof system is studied based on torque/force inputs generated by a set-point feedforward controller. The focus here is to analyze system transient and steady state response for various commands. Also of interest is tracking performance degradation due to tire compliance.

The controller is designed mainly to provide the gravity terms required to hold the three manipulator joints in static equilibrium at some desired configuration. This set of gravity torques is computed off-line and added to the feedback controller, shown in Figure 8. This controller is basically a PD type controller with gravity compensation, for improved tracking and for reducing the static errors.

As shown in Figure 8, the 3×1 gravity compensation vector $\hat{G}$ is evaluated at the 3×1 set-point vector $\hat{\mathbf{q}}_d$, which includes desired swing, boom, and stick angles. However, $\hat{G}$ is a function of all the dofs $\mathbf{q}$, and therefore, nominal roll, pitch, bounce and pendulum angle values are used. Due to this approximate computation of the gravity term $\hat{G}$, it is expected that the steady-state error given by

$$\boldsymbol{E}_{ss} = \hat{\mathbf{q}}_d - \hat{\mathbf{q}}_{ss} \tag{36}$$

will be small but not exactly zero, even if all system parameters are exactly known.

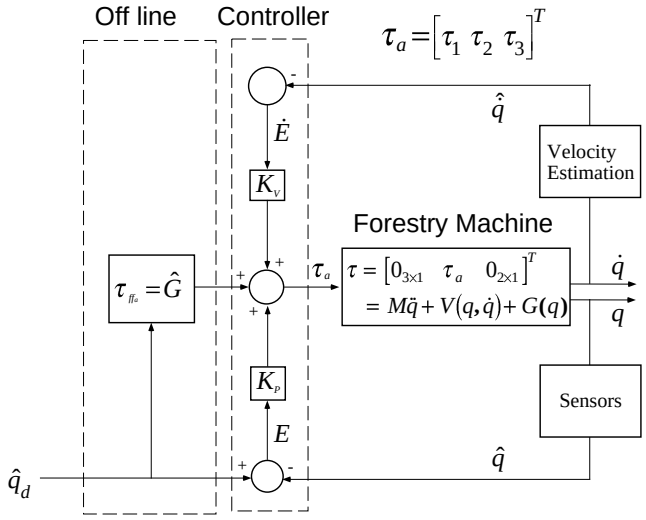

Figure 8. Set-point Feedforward Controller.

The elements of the diagonal control matrices K_P, and K_V, shown in Figure 8, are computed by

$$k_{P_i} = \omega_i^2 m_{ii} = (2\pi\nu_i)^2 m_{ii} \qquad \text{i = 1,2,3} \qquad (37a)$$

$$k_{V_i} = 2\zeta_i \omega_i m_{ii} = 4\pi\zeta_i \nu_i m_{ii} \qquad \text{i = 1,2,3} \qquad (37b)$$

where m_{ii} corresponds to diagonal elements of the mass matrix, ζ is the damping ratio, and ν the frequency of the controller. Finally, the equation for the applied torques is given by,

$$\tau_i = k_{P_i} e_i + k_{V_i} \dot{e}_i + \tau_{ff_i} \qquad \text{i = 1,2,3} \qquad (38)$$

where τ_{ff_i} is the gravity compensation feedforward term. Note that this controller is not applicable as such, since in general, in a hydraulic system it is not possible to specify actuator torques/forces. However, it can be used to evaluate the developed models, and result in better understanding of system behavior.

The simulations that follow are performed with the initial values and gains given in Table II. The system is commanded to move from a initial configuration to a final one. The errors are approximately critically damped. Additional details about the various parameters can be found in [6].

Table II. Simulation Parameters.

	Swing	Boom	Stick
Init. position, q_i (^{o})	0	0	0
Des. position, q_d (^{o})	10	-10	-10
Damping, ζ	1	1	1
Frequency, ν (*Hz*)	.15	.34	.34
Position Gain (k_p)	93997	564595	173207
Velocity Gain (k_v)	199469	528577	162158

Figure 9 (a, b, and c) shows typical actuator applied torques for a set-point command in the swing, boom, and stick angles, $\hat{\mathbf{q}}_d$. Note that these are smooth, and therefore valid actuator torques. Figures 10 (a, b, and c) depict joint tracking error performance. The observed overshoot occurs because of dynamic coupling, and because the feedforward gravity term is computed at the desired final position only. Small non-zero steady state errors are due to the effects of base compliance, and to the lack of compensation for it.

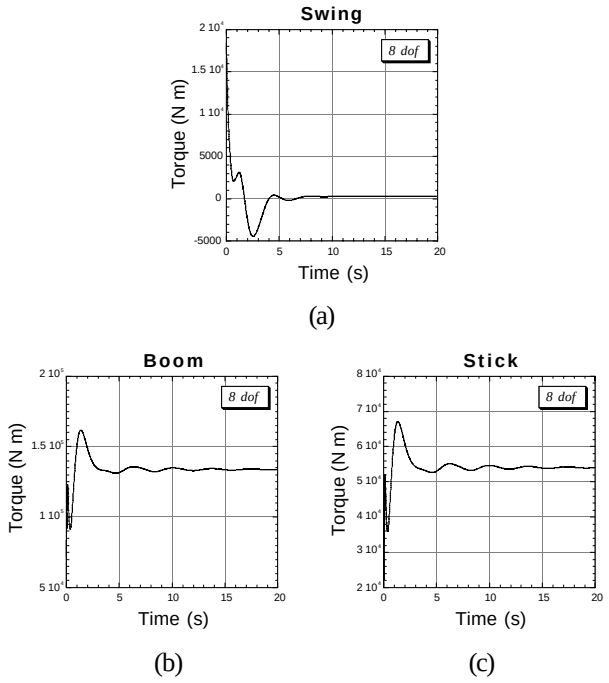

Figure 9. Applied actuator torques.

Base pitch, roll and bounce due to base compliance are depicted in Figures 10 (d, e and f). Although these are relatively small, their effect at the end-point is not negligible. This is due to the length of the manipulator arm. Finally, the angle histories of the Hooke assembly are shown in Figure 10 (g and h). As expected, since these links are not actuated, their response is quite oscillatory. However, eventually this oscillation dies out due to friction at the joints.

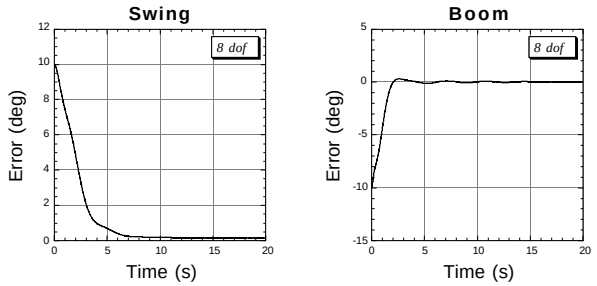

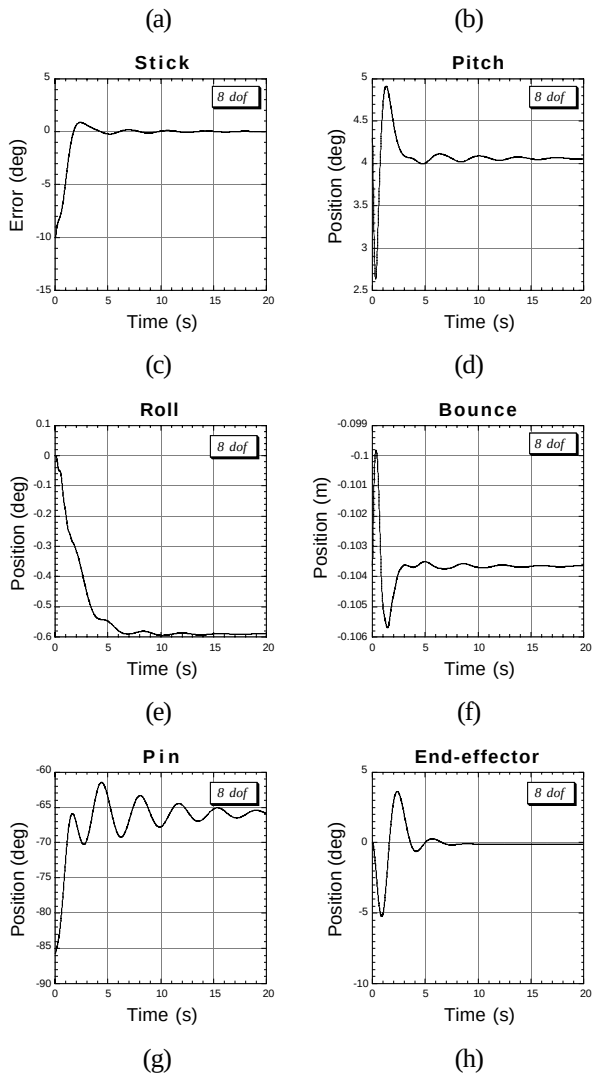

Figure 10. Transient response results.

On going work is focusing on refining the dynamic models described here, from the point of view of fidelity to the actual system. Also, the models will be incorporated in a real-time training simulator, in which speed of response will be traded-off with model detail and accuracy. In a separate paper, work on modeling the electrohydraulic subsystem, as well as on designing a coordinated controller will be presented.

7 Conclusions

This paper studied issues related to the generation of dynamic models for an electrohydraulic forestry machine. Such models can be used for training simulators, for sizing components, and for system design. The most complex model, includes base compliance, manipulator swing, boom, and stick dofs, and pendulum-like motions of the processing head, suspended from the end-point. A symbolic version of the Newton-Euler iterative method was used to include the base dofs due to the compliant tires. Techniques and experiments designed to extract system parameters were described. Based on the obtained models, a valve-sizing methodology was briefly outlined. Finally, simulation results of the machine's response were provided.

Acknowledgments

The financial support for this work by the Ministère de l'Industrie, du Commerce, de la Science et de la Technologie of Quebec, (MICST), under the program SYNERGIE is gratefully acknowledged. Also, the authors wish to thank R. Frenette (CRIM & McGill), P. Freedman (CRIM), B. Mu (McGill), J. Courteau and I. Makkonen (FERIC), R. Germain, M. Delegrave and J. LeBrun (Denharco), and D. Éthier, and R. Lessard (Autolog) for their invaluable help in various aspects of this work.

References

[1] Courteau, J., "Robotics in Canadian Forestry," *IEEE Canadian Review*, Winter 1994, pp. 10-13.

[2] Lawrence, P.D. et al, "Computer-Assisted Control of Excavator-Based Machines," *SAE Technical Paper* # 932486, Warrendale, PA, 1993.

[3] Sepehri, N. et al. "Cascade Control of Hydraulically Actuated Manipulators," *Robotica*, Vol. 8, 1990, pp. 207-216.

[4] Freedman, P., Papadopoulos, E., Poussart, D., Gosselin, C., and Courteau, J, "ATREF: Application des Technologies Robotiques aux Équipements Forestiers," *Proc. 1995 Canadian Conf. on Electrical and Computer Engineering*, Montreal, PQ, Sept. 5-8, 1995.

[5] Luh, J. Y. S., Walker, M., and Paul, R. P., "On-Line Computational Scheme for Mechanical Manipulators," *J. of Dynamic Systems, Measurement and Control*, Vol. 102, 1980, pp. 69-76.

[6] Sarkar, S., "Dynamic Modeling of an Articulated Forestry Machine for Simulation and Control," *Master's Thesis*, McGill University, 1996.

[7] Craig, J. J., *Introduction to Robotics*, Second Edition, Addison-Wesley, Reading, MA, 1989.

[8] Girard, I and Freedman, P., "A Computerized Training Environment for Forestry Operators," *Proc. Robotics and Knowledge-based Systems Workshop*, Department of National Defence and the Canadian Space Agency, St. Hubert, Que., October 15-18, 1995.

[9] Wong, J. Y., *Theory of Ground Vehicles*, John Wiley and Sons, Inc., New York, NY, 1993.